ACS APPLIED MATERIALS & INTERFACES

Research Article

www.acsami.org

Highly Efficient Photoelectrochemical Hydrogen Generation Using a Quantum Dot Coupled Hierarchical ZnO Nanowires Array

Heejin Kim and Kijung Yong*

Surface Chemistry Laboratory of Electronic Materials (SCHEMA), Department of Chemical Engineering, Pohang University of Science and Technology (POSTECH), Pohang, North Gyeongsang 790-784, Korea

Supporting Information

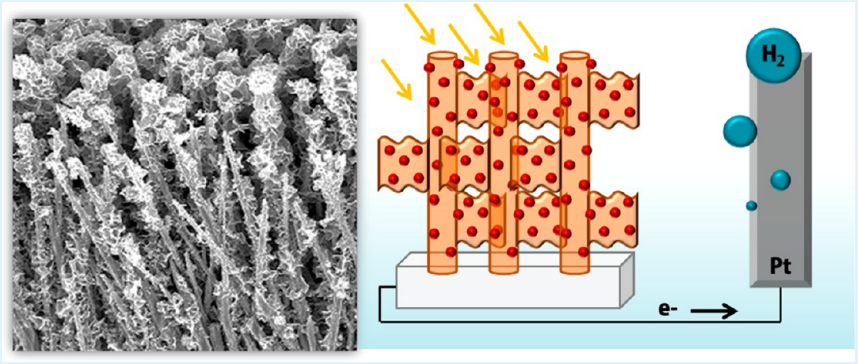

ABSTRACT: A highly efficient photoelectrochemical cell was developed using a quantum dot semiconductor coupled hierarchical ZnO nanostructure for hydrogen generation. The hierarchical ZnO nanostructure consists of ZnO nanowire as a core and 2-dimensional ZnO nanosheets shelled on the ZnO nanowire surface. This multi-dimensional nanostructured photoanode was optimized with solution process conditions for efficient charge separation and transportation, and the visible light harvesting was effectively enhanced using the low bandgap semiconductor cadmium chacogenide quantum dots. Our hierarchical ZnO nanowire photoelectrode has greatly improved the saturated photocurrent density (17.5 mA/cm^2) at 0.4 V vs. RHE under 1 sun illumination condition. In addition, we have modified the photoelectrode with $IrO_x{\cdot}nH_2O$ deposition to enhance the photostability, showing a noticeable improvement in steady generation of photocurrent under the light illumination condition.

KEYWORDS: *hierarchical nanostructure, photoelectrochemical, hydrogen, quantum dot, ZnO, CdS, CdSe*

INTRODUCTION

Recently, the demands of a renewable energy source have been of wide interest due to a serious energy crisis and environmental pollution. As a renewable and clean energy source, hydrogen is attractive as a clean fuel source because of its high energy density and abundant, sustainable properties. Recently, a photoelectrochemical (PEC) cell has been widely investigated as a promising hydrogen generation technology through the photoelectrolysis of water using abundant solar energy.[1−5] For the efficient hydrogen generation in the PEC system, the effective absorption of sunlight and rapid spatial separation of the photogenerated electron hole pairs are essential. Thus, the PEC cell should be designed to have the capability of full light harvesting and long-lasting photogenerated charges in separate states. To meet these requirements, the optimization of the materials and structure of the photoelectrode in the PEC hydrogen generation system is crucial. Therefore, tremendous efforts have been devoted to the design of suitable nanostructured photoelectrodes.[2,6]

One-dimensional nanostructures, such as nanorods,[8−12] nanowires,[13] and nanotubes[14−16] are promising candidates for achieving high performance in the PEC because these structures can enhance the charge separation and transportation with their vectored electron movements. In particular, a ZnO nanowire array has been applied to PEC cells because of the ZnO nanowire array's high electron mobility properties (up to approximately 1000 cm^2 V s^{-1} for a single ZnO nanowire)[17] and its morphology, which lowers the charge carrier loss at the grain boundaries. In addition, ZnO has a favorable band-edge position that straddles the redox potential of photoelectrolysis in water splitting. However, the overall solar conversion efficiency of a ZnO photoanode containing nanowires, especially in the PEC system, is limited compared to mesoporous films, primarily because of insufficient specific surface area for the water splitting reactions. To overcome this disadvantage, various hierarchical ZnO nanowire structures combining multiscale configurations, such as branched nanowires and nanoflowers, have been proposed to enlarge the

Received: September 27, 2013
Accepted: November 25, 2013
Published: November 25, 2013

specific surface area of the photoelectrodes.[18−24] For example, Yang et al. reported on the production of PEC cells containing secondary branched ZnO nanotetrapods with nitrogen doping, and the optimized cell showed an enhanced solar-to-electrical conversion efficiency.[25] Similarly, a CdS-deposited ZnO urchin-like hierarchical nanostructure has been used in PEC cells for hydrogen generation. Although efforts to use hierarchical ZnO photoanodes have improved the generation of photocurrents, the highest value attained has been 12 mA/cm^2.[26] Considering that the theoretical maximum photocurrent density is approximately 22 mA/cm^2 for the CdSe sensitizing system, the attained values of the photocurrent density remain low.[27] For this reason, the optimized nano-designed photoelectrode with wide range light harvesting properties is necessary for the enhanced hydrogen evolution properties.

To meet these challenges, we have applied three strategies: (i) a hierarchical nanostructured photoelectrode for efficient charge collection and transportation, (ii) multi-bandgap quantum dot cosensitizers for tunable solar light absorption capabilities with a suitable solar spectrum, and (iii) $IrO_x{\cdot}nH_2O$ hole scavenger modification to solve the low stability of quantum dot sensitizers. Specifically, we have synthesized a multi-dimensional hierarchical ZnO nanostructure using a low temperature hydrothermal method and used it as a photoelectrode in a PEC cell to achieve efficient hydrogen generation. Our hierarchical ZnO nanostructure consists of a nanosheet-shelled nanowire. This combined nanosheet and nanowire structure utilizes both a high surface area from the nanosheet and efficient charge transfer along the nanowire. In addition, this unique multi-dimensional hierarchical ZnO nanostructure enhances light absorption through light scattering effects. A CdS/CdSe quantum dot cosensitization was used as a visible light harvesting antenna. Our optimized PEC system with a multi-dimensional ZnO hierarchical nanostructure has generated a greatly enhanced saturated photocurrent density of 17.5 mA/cm^2 at 0.4 V vs. RHE. This value is the highest photocurrent density reported thus far in the PEC hydrogen generation system.

EXPERIMENTAL SECTION

Fabrication of Multi-Dimensional ZnO Nanostructure Based PEC Photoelectrode. Firstly, ZnO nanowire arrays were prepared by an all-solution process using the hydrothermal method according to a previous report.[28] A 50 nm ZnO seed layer was deposited on the cleaned FTO glass by sputtering a ZnO target at room temperature. After that, the ZnO sputtered FTO substrates were immersed in a 10 mM $Zn(NO_3)_3{\cdot}6H_2O$ (98%, Aldrich) aqueous solution in which the pH had been adjusted to 11 by adding ammonia (28 wt % in water, Aldrich), and the solution was heated at 95 °C overnight. The nanowire length was controlled over 10 μm length through growth time. After the NW growth process, the substrate was removed from the solution, rinsed with deionized (DI) water, and then dried using blown nitrogen. Second, the ZnO nanowire arrays were transferred into the aqueous solution with equal molecules of 10 mM $Zn(NO_3)_3{\cdot}6H_2O$, hexamethylenediamine ($C_6H_{16}N_2$, Aldrich), and 1 mM trisodium citrate ($C_6H_5Na_3{\cdot}2H_2O$, Aldrich), and the solution was heated at 70 °C with various growth times.[29] The obtained multi-dimensional ZnO nanostructures were optimized with various secondary reaction times.

CdSe/CdS/ZnO NW arrays were prepared by a three-step solution based method according to a previous report.[30] The prepared ZnO nanostructures were in situ sensitized with CdS and CdSe using a successive ionic layer absorption and reaction (SILAR) and chemical bath deposition (CBD), respectively. The samples were dipped in 200 mM $CdSO_4$ for 30 s, rinsed with deionized water for 30 s, dipped for another 30 s in 200 mM aqueous Na_2S, and rinsed with water for 30 s. All these processes constitute one SILAR cycle and are repeated for 20 cycles in order to get a suitable CdS loading on the ZnO NWs. CdSe was in situ deposited on the CdS/ZnO NWs by CBD. The samples were immersed in an aqueous solution containing 0.5 mmol of $Cd(CH_3COO)_2$ $2H_2O$, 0.25 mmol of Na_2SeSO_3, and 150 μL of ammonium hydroxide solution in 20 mL of deionized water for 3−4 h at 95 °C. The CBD process was also repeated for 3 cycles.

The deposition process of the $IrO_x{\cdot}nH_2O$ on the CdSe/CdS/ZnO surface was performed according to previous work.[31] Briefly, the colloidal $IrO_x{\cdot}nH_2O$ aqueous solution was prepared by hydrolysis of 2 mM Na_2IrCl_6 at pH 13. After the reaction time of 20 min at 90 °C, the acid condensation process was conducted using 3 M HNO_3 in an ice bath for 80 min. After that, the pH of the solution was adjusted to 6.8, and then, the CdSe/CdS/ZnO nanostructure arrays were immersed in the prepared $IrO_x{\cdot}nH_2O$ for 40 min. Then, the electrode was washed with deionized water and dried at 100 °C for 12 h.

Characterization. Scanning electron microscopy (SEM) images were recorded using a Phillips XL30S field emission SEM. An atomic scale analysis of the crystal structure was performed on a transmission electron microscope (JEM-2200FS, JEOL at NCNT, POSTECH) equipped with an EELS (electron energy loss spectroscopy) elemental mapping (EF-TEM). The optical absorbance of the samples was analyzed using a UV2501PC (SHIMADZU) spectrometer with an ISR-2200 integrating sphere attachment for diffuse reflection measurements. The photocurrent density−voltage characteristics of the photoelectrochemical cells were measured under a simulated air mass 1.5 G solar spectrum. The intensity was adjusted to 100 mW/cm^2 using an NREL-certified silicon reference cell equipped with a KG-5 filter. Photocurrent−voltage (I−V) measurements were performed using a typical three-electrode potentiostat system (potentiostat/galvanostat, model 263A, EG&G Princeton Applied Research) with a Pt counter electrode and a saturated calomel reference electrode (SCE). An aqueous solution containing 0.25 M Na_2S and 0.35 M Na_2SO_3 was used as the electrolyte through which nitrogen was bubbled, and the working electrode was illuminated from the front side with a solar-simulated light source (AM 1.5 G filtered, 100 mW/cm^2, 91160, Oriel). The hydrogen evolution test was conducted in a 5 cm diameter and 115 cm^3 volume capacity three-neck apparatus for a 6000 s time duration. The evolved hydrogen was measured at 20 minute intervals. The evolved amounts of H_2 were analyzed by a gas chromatograph (HP5890) with a thermal conductivity detector (TCD) and a molecular sieve 5-A column.

RESULTS AND DISCUSSION

Development of CdSe/CdS Cosensitized 3-Dimensional ZnO Nanostructure. One of the approaches to increase the surface area of ZnO nanowire photoelectrodes for improved solar to hydrogen conversion efficiency is to fabricate hierarchical ZnO nanowire structure. For this purpose, the hierarchically shelled ZnO nanowire structures were prepared by secondary growth on the ZnO nanowire arrays using a low temperature solution process. For the lateral growth in the secondary process, the citrate ions were mainly used in growth solution. Using this process, the 2-dimensional ZnO nanosheets were successfully deposited along the ZnO nanowire surface. During the second growth stage, citrate ions in the precursor solution inhibit the c-axis growth of ZnO while ZnO nuclei adsorb on the ZnO nanowire surface. Subsequently, the absorbed ZnO nanocrystals act as new sites for ZnO nuclei adsorption, resulting in forming 2-dimensional ZnO nanosheets. Over the period, the aggregation of ZnO nanoparticles proceeds to form the 2-dimensional ZnO nanosheets, which shell around the ZnO nanowire surface.

This morphological evolution of the hierarchical ZnO nanostructure was investigated by increasing the reaction time of the secondary growth and observing the changes in the ZnO

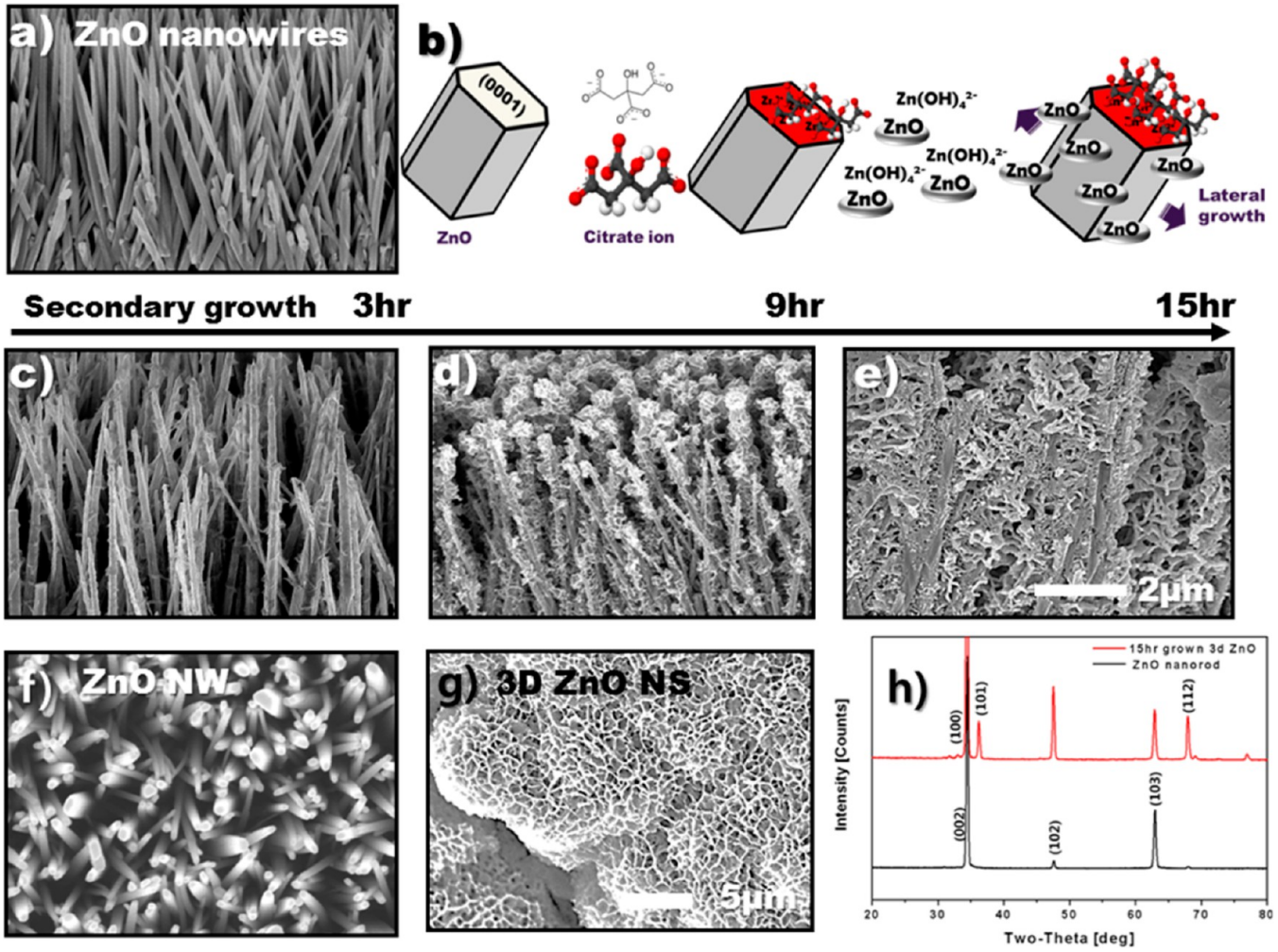

Figure 1. (a, c–e) Cross-sectional SEM images of the ZnO nanostructure array grown over varying reaction times. (a) Pristine ZnO nanowire arrays after the first growth process. (b) Schematic illustration of the secondary growth process. Hierarchical ZnO nanowires after (c) 3 h, (d) 9 h, and (e) 15 h secondary growth. Top view images of (f) bare ZnO nanowires and (g) 15 h grown 3D nanostructure and (h) corresponding XRD patterns.

nanowires' morphology. Figure 1a,c–e shows the SEM images of the ZnO nanostructure arrays on the FTO after secondary growth for different reaction times. Initially, high, dense, and vertically aligned ZnO nanowires with over ~10 μm length and 80–100 nm diameter were prepared on the FTO substrate, as shown in Figure 1a. After the secondary growth, the ZnO nanowire surface became rough and bumpy due to the secondary grown 2-dimensional ZnO nanosheet. For the secondary growth, the ZnO nanowire-covered FTO glass was immersed in a citrate ion solution at a reaction temperature of 70 °C for various growth times. Figure 1c–e demonstrates the growth of the nanosheets along the backbones of the ZnO nanorods with increased reaction time. The growth mechanism of the nanosheets is strongly dependent on the citrate ions in the solution reaction. Basically, the ZnO has a top polar zinc (001) face with size symmetric nonpolar {100} planes parallel to the [0001] direction. In secondary process, the electro-positively charged, Zn-terminated ZnO (001) top plane favors the chemisorption of the negatively charged citrate ions, suppressing the c-axis growth of the ZnO but causing growth on the nonpolar ZnO side-planes.[23,32] Under this condition, the ZnO nuclei preferentially adsorb on the sidewall surface of the ZnO nanowires, and subsequently, the absorbed ZnO nano-crystals act as accommodation sites for the ZnO nuclei adsorption, resulting in the formation of the hierarchical ZnO nanostructure (Figure 1b).

During the secondary growth period, the ZnO nanoparticles aggregate to form the 2-dimensional ZnO nanosheets, which form a shell around the ZnO nanowire surface. Figure 1c clearly shows the nanoparticles' growth on the ZnO nanowire surface, and Figure 1d,e demonstrates the subsequent growth of the two-dimensional ZnO nanosheets covering the overall ZnO nanowire arrays with increased reaction time. Figure 1f,g shows the SEM top view images of the pristine ZnO nanowires and hierarchical ZnO nanostructure obtained after a 15 h secondary growth. The hierarchical ZnO nanowire is fully enclosed by two-dimensional ZnO nanosheets by forming a network throughout the top surface. Compared to the ZnO nanowires, which have a c-axis preferential growth direction, the multi-dimensional ZnO nanostructures have a polycrystalline nature, as confirmed by the X-ray diffraction (XRD) patterns shown in Figure 1h. The XRD patterns of the multi-dimensional ZnO nanostructures reveal that polycrystalline ZnO nanosheets were grown on single crystalline hexagonal ZnO nanowires with atomic plane spacings corresponding to the JCPDS No.79-2205 (ZnO). The additional XRD peaks at (101) and (112) were obtained from the nanosheet shell around the ZnO nanowires, having a main peak at (002).

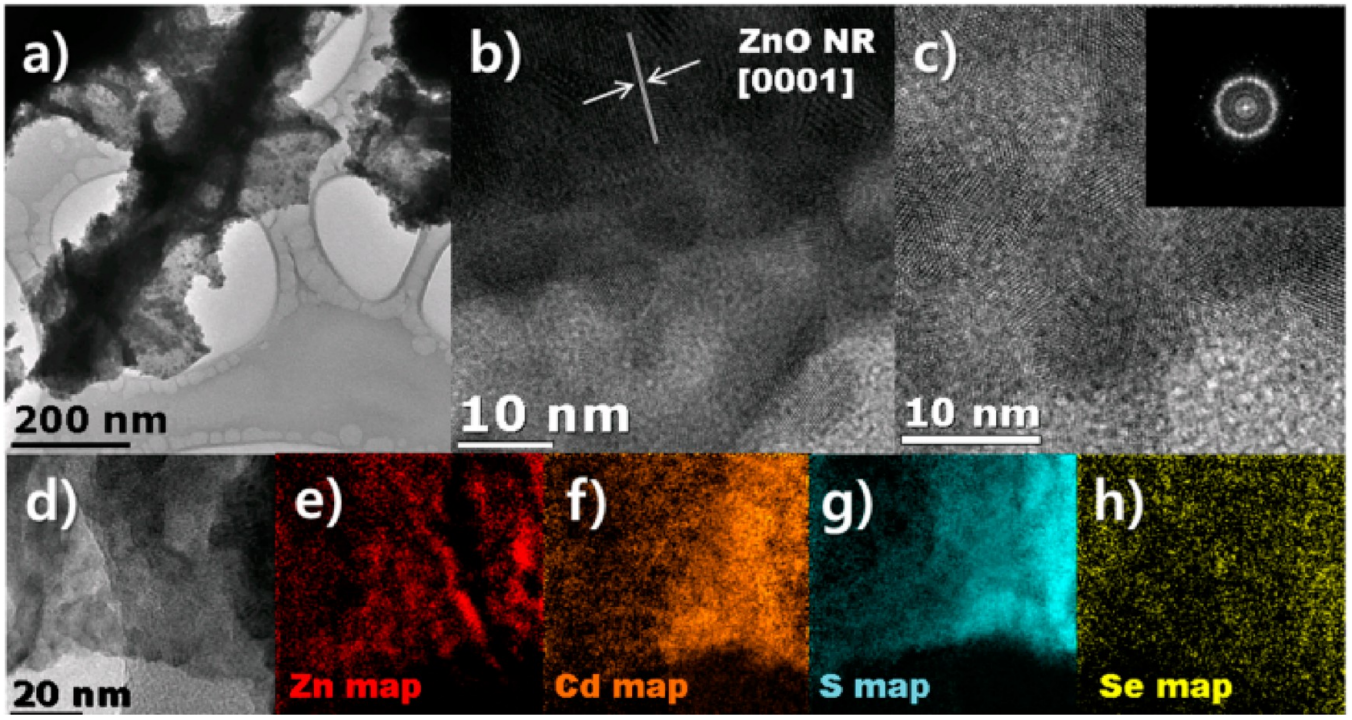

Figure 2. TEM images of CdSe/CdS deposited 9 h grown ZnO nanostructure (a) low magnified TEM image and (b) HRTEM image at the interface of CdSe/CdS deposited nanosheet shelled on the ZnO nanowire surface and (c) HRTEM image of CdSe/CdS/ZnO nanosheet with the corresponding FFT pattern. (d–h) HRTEM image and corresponding EELS mapping images (Zn, Cd, S, Se elements) of the CdSe/CdS/ZnO nanosheet.

Because the ZnO can only absorb light in the UV region due to its wide bandgap (approximately 3.27 eV), the hierarchically shelled multi-dimensional ZnO nanostructure is often coupled with narrow bandgap materials to enhance its visible light absorption capability. We have used narrow bandgap cadmium chacogenide quantum dots, CdS, and CdSe QDs, as cosensitizers because they have narrow bandgap value which absorb visible light. The QDs were deposited through a low-temperature solution process. First, the CdS shell was formed on the hierarchical ZnO nanostructure surface using the SILAR (successive ionic layer absorption reaction) process with an adequate number of repeated cycles (~20) to create a shell thickness of approximately 10 nm. This layer-by-layer self-limiting growth nature of the SILAR is useful in forming a conformal coating on the hierarchical nanostructure. Subsequently, the CdSe quantum dots were uniformly deposited on the CdS/ZnO nanostructure with the CBD (chemical bath deposition) process. We performed HR-TEM analysis to demonstrate the successful loading of cadmium chacogenide QDs on the multi-dimensional ZnO nanostructure surface. After the CdSe/CdS QDs were deposited, small dots were distributed all over the ZnO nanostructure surface, as observed in the low magnification TEM image (Figure 2a). The HRTEM image of the interface of the nanowire and nanosheet shows that the CdS and CdSe QDs were loaded uniformly on the 3D hierarchical ZnO nanostructure surface (Figure 2b). In addition, the HRTEM images of the ZnO nanosheet in Figure 2c,d confirmed the polycrystalline nature of QDs grown on the ZnO nanosheet. Furthermore, the EELS mapping indicated that the Zn, Cd, S, and Se elements were equally distributed throughout the ZnO surface (Figure 2e–h).

Photoelectrochemical (PEC) Cell Performance for Hydrogen Generation. For further analysis in optical properties, the light absorbance analysis was conducted with pristine ZnO nanostructure, CdS/ZnO nanostructure, and CdSe/CdS/ZnO nanostructure. As observed in Figure 3a, the pristine ZnO only absorbs the UV region with correlation to its optical bandgap of 3.27 eV. With the CdS SILAR process, the color of ZnO changed to yellow from white. This can be further observed by absorption spectra of the CdS/ZnO nanostructure with an absorption edge of ~540 nm which correlates with the CdS bandgap value (~2.4 eV). After the CdSe quantum dot deposition process, the color of electrodes was changed to red–brown from yellow by the naked eye. In the absorption spectra, the absorption edge of the CdSe/CdS deposited ZnO nanostructures shows an absorption edge at the wavelength of about ~700 nm corresponding to the absorption of CdSe and CdS quantum dots on ZnO nanostructures (CdS: 2.4 eV; CdSe: 1.7 eV).[20] The CdSe/CdS QD-modified 3-D ZnO nanostructure can be used as an efficient photoelectrode in a PEC hydrogen generation system because this structure has the advantages of a large surface area, efficient charge transfer with type II bandgap alignment, and visible light harvesting capability. The photocurrent density measurements were performed in a three-electrode cell using the 3-D CdSe/CdS/ZnO nanostructure as the working electrode with various secondary time, a Pt mesh as the counter electrode, and a saturated calomel reference electrode in a 0.35 M Na_2SO_3 and 0.25 M Na_2S electrolyte. In this experiment, the polysulfide electrolyte was used as a sacrificial reagent for consuming the remaining holes at the photoelectrode.[33,34] The photocurrent density versus the applied voltage scan of the samples was measured under visible light irradiation in the 1 sun condition. The results are presented in Figure 3b. For the accurate comparison with specific surface area of photoelectrode, four different types of CdSe/CdS QD-modified ZnO nanostructures

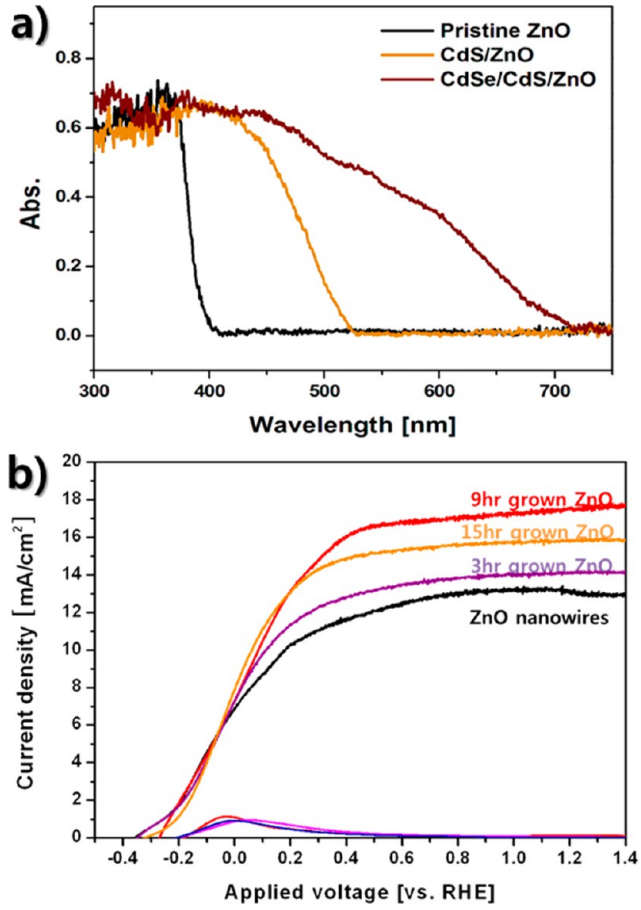

Figure 3. (a) Absorption spectra of the pristine 3D ZnO nanostructure, CdS modified 3D ZnO nanostructure, and CdSe/CdS deposited 3D ZnO nanostructure on FTO substrate. (b) Current density versus potential for QD sensitized ZnO nanostructures (20 cycles of CdS deposition/3 cycles of CdSe deposition) under illumination of AM 1.5 light at 100 mW/cm^2 (cell area 5 mm × 5 mm).

were tested as photoanodes, including pristine CdSe/CdS/ZnO nanowires and the CdSe/CdS/3-D ZnO nanostructures fabricated with secondary growth times of 3, 9, and 15 h. As expected, compared to the saturated photocurrent of 13 mA/cm^2 generated by the pristine ZnO nanowire array, the photoanodes composed of the 3-D ZnO nanostructure produced an enhanced photocurrent density. As shown in Figure 3b, a higher saturated photocurrent was obtained with a higher secondary growth time of up to 9 h, whereas the photocurrent slightly decreased for the sample with a 15 h secondary growth time. The maximum saturated photocurrent density of 17.5 mA/cm^2 was obtained for the CdSe/CdS/3-D ZnO nanostructure photoanode grown for 9 h, which generated a photocurrent density of 8 mA/cm^2 at 0 V vs. RHE. This saturated photocurrent density is comparable to the previous PEC studies. Table 1 summarizes PEC performance parameters obtained from various metal oxide nanostructured photoelectrodes sensitized with QDs, and the results showed the saturated photocurrent density ranging from 1.5 to 16 mA/cm^2.[19,21,26,35−37] Compared to these results, our CdSe/CdS QD-modified 3D ZnO photoanode generated the highest photocurrent density among QD-modified metal oxide photoelectrodes. Furthermore, we have additionally calculated the solar to hydrogen efficiency (STH) with two electrode systems

Table 1. Photoelectrochemical Performance Using Quantum Dot Light Sensitized Photoelectrodes

structure	photosensitizer	saturated current density, mA/cm^2
CdSSe/ZnO nanowire arrays[35]	CdSSe	6
CdSe/ZnO textured porous film[19]	CdSe	4.3
CdS/ZnO urchin-like hierarchical nanostructure[26]	CdS	12
PbS/TiO_2 mesoporous film[39]	PbS	1.5
CdS/TiO_2 inverse opals[6]	CdS	4.84
$CuInS_2$/CdS/TiO_2 mesoporous film[41]	$CuInS_2$/CdS	16
CdSe/CdS/TiO_2 heterostructure[36]	CdSe/CdS	6
PbS/CdS/TiO_2 mesoporous film[37]	PbS	6
CdSe/CdS ZnO nanowire arrays[a]	CdSe/CdS	13
CdSe/CdS ZnO 3D nanostructures[a]	CdSe/CdS	17.5

[a]Results in this study.

(Figure S1 in the Supporting Information). The optimized CdSe/CdS/3D ZnO photoelectrodes showed the maximum STH value of 2.45% at 0.2 V.

The enhanced photocurrent density of the hierarchical ZnO nanostructure is primarily attributed to the increased surface area of the 2-D nanosheet-shelled ZnO nanowire structure, which enables a higher CdSe/CdS QD loading compared to bare ZnO nanowires. In addition, the hierarchical nanostructure effectively captures the incident light with a light scattering effect, and the ZnO nanowire in the core facilitates the rapid charge transport through a direct electron pathway. These combined factors play a key role in enhancing the efficiency of solar energy conversion. The optimum 3D ZnO nanostructure photoanode was obtained with a secondary growth of 9 h because a longer reaction time (such as 15 h) creates a network of nanosheets, as seen in Figure 1e,g, which allows small pore sizes to hinder the QD loading throughout the nanowire array.

In addition to the generation of high photocurrent, the photostability of the electrodes is another key factor for the development of an efficient PEC hydrogen generation system. Thus, we tested the stability of the photoanodes using chronoamperometric measurements at 0 V vs. SCE. Upon illumination of the sample at 100 mW/cm^2, the current density was monitored over time, and the results are shown in Figure 4a. In this measurement, both the CdSe/CdS QD-modified 1-D and 3-D ZnO nanostructure photoanodes showed a gradual decrease in the photocurrent by more than 35% after a 6000 s operation. This decrease occurred due to the low stability of cadmium chacogenide under light illumination. The reason for this low stability originates from the hole accumulation at the QDs in operation, which results in the photocorrosion of the QDs. To improve the photostability of the QDs, we used $IrO_x \cdot nH_2O$ passivation of the surface of the QDs. In previous research, we have successfully modified the CdSe/CdS/ZnO surface with $IrO_x \cdot nH_2O$. The modified thin and well-spread $IrO_x \cdot nH_2O$ nanoparticles provided efficient hole scavenging from the quantum dots, which enhances the charge separation process.[31,38] In terms of photostability, the $IrO_x \cdot nH_2O$, a well-known oxygen-evolution catalyst, can also effectively scavenge the holes, resulting in suppression of the hole-induced anodic corrosion of the cadmium chacogenide QDs. In addition, the $IrO_x \cdot nH_2O$ can retard the interfacial recombination between electrons in the conduction band of the ZnO and the holes

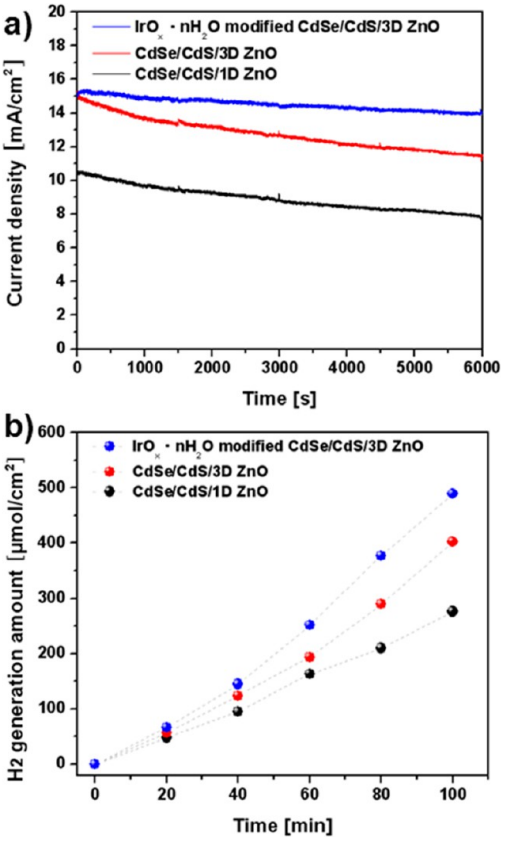

Figure 4. (a) Current density versus time at zero bias (vs. SCE) for QD-sensitized 3D ZnO nanostructures under an illumination of AM 1.5 light at 100 mW/cm^2 and (b) gas chromatography mass spectroscopy (GC-MASS) plot of the evolved gas versus time under the same conditions of (a).

remaining in the QDs by passivating the surface states. Thus, the $IrO_x{\cdot}nH_2O$ modified photoanode efficiently inhibited hole accumulation in the charge separation process, and this eventually improved the photostability. To understand how the electrode works, a schematic diagram of the $IrO_x{\cdot}nH_2O$ modified CdSe/CdS/3D ZnO nanostructure was shown in Scheme 1. As depicted, the 3D ZnO nanostructures efficiently capture the incident light and CdS/CdSe semiconductor QDs generate the photoexcited electron hole pairs. The deposited $IrO_x{\cdot}nH_2O$ scavenges the remaining holes on the sensitizer surface by reacting in sacrificial reagent. As shown Figure 4a, the $IrO_x{\cdot}nH_2O$-modified photoelectrode showed a greatly improved photostability, indicating only an approximately 15% decrease in photocurrent after a 6000 s operation under illumination. Also, the measured photocurrent density is comparable with unmodified photoelectrode because the $IrO_x{\cdot}nH_2O$ effectively participates in charge separation by lowering the recombination rate at the quantum dot interface.[31] In addition to photostability, we measured the generation of real hydrogen gas at a potential of 0 V vs. SCE which is the starting point of the saturated photocurrent. The measurement condition in the hydrogen evolution test is done at the applied voltage of photocurrent density up to 17.5 mA/cm^2. As shown in Figure 4b, the evolved hydrogen gas was collected and analysed using gas chromatography. The measured hydrogen evolution showed a faradic efficiency greater than 90%. The difference of about 10% from the ideal value (100%) is thought to be due to the recombination of charges at the interface while reducing water at the Pt cathode. In this work, the rate of hydrogen generation was measured by gas chromatography-mass spectrometry at zero bias (vs. SCE) under 1 sun illumination condition.[6,7] Our PEC system produced an average hydrogen evolution rate of 239 μmol·h^{-1}cm^{-2}. These results are comparable with the previous PEC outcomes for hydrogen generation in similar quantum dot sensitized systems. Tada et al. reported a hydrogen production rate of 5.2 mL·h^{-1} using PbS sensitized mesoporous TiO_2 film.[39] They also reported a Ag_2S QD sensitized PEC system yielding H_2 at a rate of 0.8 mL·h^{-1} with a total conversion efficiency of 0.29 %.[40] Recently, the CdS quantum dot sensitized TiO_2 inverse opals have generated a maximum photocurrent density of 4.84 mA cm^{-2}.[21] Teng et al. also developed the CdS/$CuInS_2$/TiO_2 PEC cells for hydrogen generation with 16 mA cm^{-2} photocurrent density.[41] In addition, the QD sensitized TiO_2 heterostructure using CdS/CdSe quantum dot has also shown 80 mL·cm^{-2}·day^{-1} H_2 generation,[36] and the PbS sensitized TiO_2 system has achieved infrared light harvesting with 4.30 ± 0.25 mL·cm^{-2}·day^{-1}

Scheme 1. Schematic Diagram of the Hierarchically Shelled CdSe/CdS/ZnO Nanostructure Electrode Modified with $IrO_x{\cdot}nH_2O$ and Its Energy Gap Structure in the Hydrogen Generation Process

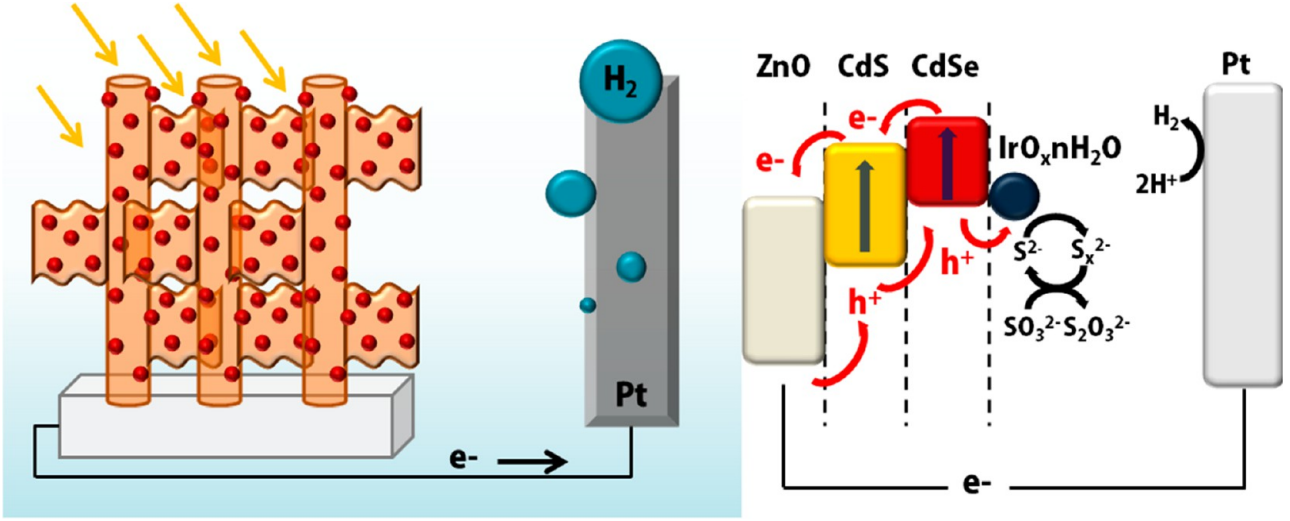

dx.doi.org/10.1021/am404259y | ACS Appl. Mater. Interfaces 2013, 5, 13258−13264

hydrogen production.[37] Compared to these results, our PEC cells showed an enhanced photocurrent density with promising hydrogen generation rates.

CONCLUSION

In summary, we have developed nano-designed photoelectrochemical cells using a hierarchically shelled ZnO nanostructure consisting of a two-dimensional ZnO nanosheet shell and a ZnO nanowire core coupled with cadmium chacogenide QDs as visible light sensitizers for a PEC hydrogen generation system. The photoelectrodes were fabricated using a series of facile low-temperature solution processes. The obtained 3-D ZnO hierarchical nanostructure is an efficient PEC photoanode because the structure provides an enhanced surface area consisting of 2-D nanosheets for high QD loading, efficient charge transfer by a directional transport path through the 1-D nanowire, and effective light capturing by light scattering effects. Consequently, the PEC cell generated an unprecedented photocurrent density of 17.5 mA/cm^2 under the 1 sun illumination condition at 0 V vs. SCE bias condition. In addition, the photostability of the QDs was greatly improved by introduction of $IrO_x \cdot nH_2O$ passivation of the QD surface to retard photocorrosion.

ASSOCIATED CONTENT

Supporting Information

Solar to hydrogen conversion efficiency calculated using a two-electrode system of photoelectrochemical cells. This material is available free of charge via the Internet at http://pubs.acs.org/.

AUTHOR INFORMATION

Corresponding Author

*E-mail: kyong@postech.ac.kr.

Notes

The authors declare no competing financial interest.

ACKNOWLEDGMENTS

This work was supported by the National Research Foundation of Korea (2013-R1A2A2A05-005344).

REFERENCES

(1) Khaselev, O.; Turner, J. A. *Science* **1998**, *280*, 425−427.
(2) Minggu, L. J.; Daud, W. R. W.; Kassim, M. B. *Int. J. Hydrogen Energy* **2010**, *35*, 5233−5244.
(3) Abe, R. *J. Photochem. Photobiol., C: Photochem. Rev.* **2010**, *11*, 179−209.
(4) Choudhary, S.; Upadhyay, S.; Kumar, P.; Singh, N.; Satsangi, V. R.; Shrivastav, R.; Dass, S. *Int. J. Hydrogen Energy* **2012**, *37*, 18713−18730.
(5) Aroutiounian, V. M.; Arakelyan, V. M.; Shahnazaryan, G. E. *Sol. Energy* **2005**, *78*, 581−592.
(6) Luo, J.; Karuturi, S. K.; Liu, L.; Su, L. T.; Tok, A. I. Y.; Fan, H. J. *Sci. Rep.* **2012**, *2*, 451−456.
(7) Satsangi, V. R.; Kumari, S.; Singh, A. P.; Shrivastav, R.; Dass, S. *Int. J. Hydrogen Energy* **2008**, *33* (1), 312−318.
(8) Cho, I. S.; Chen, Z.; Forman, A. J.; Kim, D. R.; Rao, P. M.; Jaramillo, T. F.; Zheng, X. *Nano Lett.* **2011**, *11*, 4978−4984.
(9) Vanalakar, S. A.; Mali, S. S.; Pawar, R. C.; Tarwal, N. L.; Moholkar, A. V.; Kim, J. H.; Patil, P. S. *J. App. Phys.* **2012**, *112*, 044302−044307.
(10) Wang, X.; Zhu, H.; Xu, Y.; Wang, H.; Tao, Y.; Hark, S.; Xiao, X.; Li, Q. *ACS Nano* **2010**, *4*, 3302−3308.
(11) Wang, M.; Jiang, J. G.; Shi, J. W.; Guo, L. J. *ACS. Appl. Mater. Interfaces* **2013**, *5*, 4021−4025.
(12) Li, Y. B.; Takata, T.; Cha, D.; Takanabe, K.; Minegishi, T.; Kubota, J.; Domen, K. *Adv. Mater.* **2013**, *25*, 125−131.
(13) Wang, G.; Yang, X.; Qian, F.; Zhang, J. Z.; Li, Y. *Nano Lett.* **2010**, *10*, 1088−1092.
(14) Shin, K.; Seok, S. i.; Im, S. H.; Park, J. H. *Chem. Commun.* **2010**, *46*, 2385−2387.
(15) Kang, Q.; Liu, S.; Yang, L.; Cai, Q.; Grimes, C. A. *ACS Appl. Mater. Interfaces* **2011**, *3*, 746−749.
(16) Tsui, L. K.; Zangari, G. *Electrochim. Acta* **2013**, *100*, 220−225.
(17) Gonzalez-Valls, I.; Lira-Cantu, M. *Energy Environ. Sci.* **2009**, *2*, 19−34.
(18) Hwang, Y. J.; Boukai, A.; Yang, P. *Nano Lett.* **2008**, *9*, 410−415.
(19) Emin, S.; Fanetti, M.; Abdi, F. F.; Lisjak, D.; Valant, M.; van de Krol, R.; Dam, B. *ACS Appl. Mater. Interfaces* **2013**, *5*, 1113−1121.
(20) Kim, H.; Seol, M.; Lee, J.; Yong, K. *J. Phys. Chem. C* **2011**, *115*, 25429−25436.
(21) Karuturi, S. K.; Luo, J.; Cheng, C.; Liu, L.; Su, L. T.; Tok, A. I. Y.; Fan, H. *J. Adv. Mater.* **2012**, *24*, 4157−4162.
(22) Joshi, R. K.; Schneider, J. J. *Chem. Soc. Rev.* **2012**, *41*, 5285−5312.
(23) Tian, Z. R.; Voigt, J. A.; Liu, J.; McKenzie, B.; McDermott, M. J.; Rodriguez, M. A.; Konishi, H.; Xu, H. *Nat. Mater.* **2003**, *2*, 821−826.
(24) Yao, C. Z.; Wei, B. H.; Ma, H. X.; Li, H.; Meng, L. X.; Zhang, X. S.; Gong, Q. J. *J. Power Sources* **2013**, *237*, 295−299.
(25) Qiu, Y.; Yan, K.; Deng, H.; Yang, S. *Nano Lett.* **2011**, *12*, 407−413.
(26) Hieu, H. N.; Dung, N. Q.; Kim, J.; Kim, D. *Nanoscale* **2013**, *5*, 5530−5538.
(27) Li, Z.; Luo, W.; Zhang, M.; Feng, J.; Zou, Z. *Energy Environ. Sci.* **2013**, *6*, 347−370.
(28) Tak, Y.; Yong, K. *J. Phys. Chem. B* **2005**, *109*, 19263−19269.
(29) Dong, H.; Wang, L.; Gao, R.; Ma, B.; Qiu, Y. *J. Mater. Chem.* **2011**, *21*, 19389−19394.
(30) Seol, M.; Kim, H.; Tak, Y.; Yong, K. *Chem. Commun.* **2010**, *46*, 5521−5523.
(31) Seol, M.; Jang, J.-W.; Cho, S.; Lee, J. S.; Yong, K. *Chem. Mater.* **2012**, *25*, 184−189.
(32) Kim, J. H.; Andeen, D.; Lange, F. F. *Adv. Mater.* **2006**, *18*, 2453−2457.
(33) Ke, D.; Liu, S.; Dai, K.; Zhou, J.; Zhang, L.; Peng, T. *J. Phys. Chem. C* **2009**, *113*, 16021−16026.
(34) Jia, L.; Wang, D.-H.; Huang, Y.-X.; Xu, A.-W.; Yu, H.-Q. *J. Phys. Chem. C* **2011**, *115*, 11466−11473.
(35) Myung, Y.; Jang, D. M.; Sung, T. K.; Sohn, Y. J.; Jung, G. B.; Cho, Y. J.; Kim, H. S.; Park, J. *ACS Nano* **2010**, *4*, 3789−3800.
(36) Rodenas, P.; Song, T.; Sudhagar, P.; Marzari, G.; Han, H.; Badia-Bou, L.; Gimenez, S.; Fabregat-Santiago, F.; Mora-Sero, I.; Bisquert, J.; Paik, U.; Kang, Y. S. *Adv. Energy Mater.* **2013**, *3*, 176−182.
(37) Trevisan, R.; Rodenas, P.; Gonzalez-Pedro, V.; Sima, C.; Sanchez, R. S.; Barea, E. M.; Mora-Sero, I.; Fabregat-Santiago, F.; Gimenez, S. *J. Phys. Chem. Lett.* **2012**, *4*, 141−146.
(38) Zhao, Y.; Hernandez-Pagan, E. A.; Vargas-Barbosa, N. M.; Dysart, J. L.; Mallouk, T. E. *J. Phys. Chem. Lett.* **2011**, *2*, 402−406.
(39) Jin-nouchi, Y.; Hattori, T.; Sumida, Y.; Fujishima, M.; Tada, H. *ChemPhysChem* **2010**, *11*, 3592−3595.
(40) Nagasuna, K.; Akita, T.; Fujishima, M.; Tada, H. *Langmuir* **2011**, *27*, 7294−7300.
(41) Li, T.-L.; Lee, Y.-L.; Teng, H. *J. Mater. Chem.* **2011**, *21*, 5089−5098.